Characterisation of optically thin cells and experimental liquid crystals

DENITSA BANKOVA[1,*], NICOLAS BROUCKAERT[1], NINA PODOLIAK[1], BENJAMIN BEDDOES[1], ELEANOR WHITE[1], OLEKSANDR BUCHNEV[2], MALGOSIA KACZMAREK[1], AND GIAMPAOLO D'ALESSANDRO[3]

[1] School of Physics and Astronomy, University of Southampton, Southampton SO17 1BJ, United Kingdom
[2] Optoelectronics Research Centre and Centre for Photonic Metamaterials, University of Southampton, Southampton SO17 1BJ, United Kingdom
[3] School of Mathematical Sciences, University of Southampton, Southampton SO17 1BJ, United Kingdom
[*] Corresponding author: d.o.bankova@soton.ac.uk

Compiled May 20, 2022

The current development of new liquid crystal devices often requires the use of thin cells and new, experimental materials. Characterising these devices and materials with optical methods can be challenging if (1) the total phase lag is small ("thin cells") or (2) the liquid crystal optical and dielectric properties are only partially known. We explore the limitations of these two challenges for efficient characterisation and assessment of new liquid devices. We show that it is possible to extract a wealth of liquid crystal parameters even for cells with a phase lag of $\Delta\Phi \approx \pi$, such as E7 liquid crystal in a $1.5\,\mu m$ cell, using cross-polarised intensity measurements. The reliability of the optical method is also demonstrated for liquid crystals without precise values of the dielectric or refractive index coefficients.

http://dx.doi.org/10.1364/ao.XX.XXXXXX

1. INTRODUCTION

Thin liquid crystal (LC) cells are popular in industry, for example, paper-thin displays [1], paper-like displays [2], plastic sheet liquid-crystal displays (LCDs) [3], and ultrathin LCs for augmented reality and virtual reality [4]. Optically thin LC cells with low birefringence are also used as active-matrix LCDs [5] and thin spatial phase modulators for THz applications [6].

Apart from the device thickness, the desired modulation of light is typically achieved by selecting appropriate LCs and alignment layers. The LC materials can include, for example, experimental mixtures or, increasingly often, colloidal suspensions of inorganic or plasmonic nanoparticles in LCs [7–12]. The physical, electrical or optical properties of such mixtures differ from the ones of the LC host, so they need to be recharacterised. This can also be an issue when newly synthesised, experimental liquid crystals are used. Typically, only the birefringence or the dielectric anisotropy is known, but not the actual values of the refractive indices or the dielectric coefficients. This then leads to the question of how this partial knowledge affects the measurement of the other liquid crystal properties.

There are several methods for measuring LC properties, such as Fréedericksz transition [13], Rayleigh light scattering [14], free energy perturbations [15], nonlinear effects [16] and birefringence [17, 18]. Most of these methods, however, are not able to measure multiple parameters in a single experiment for thin cells. For example, the pretilt angle in 4.5 µm cells was measured with capacitance-voltage methods using previously known liquid crystal parameters [19]. In 2.4 µm-thick reflective liquid crystal on silicon cells with thick alignment layers pretilt angle, anchoring energy and effective birefringence were determined by fitting voltage-dependent reflectance curves [20].

Here we show a method based on the use of a single cross-polarised intensity (CPI) measurement of planar LC cells to provide an accurate estimation of the device parameters in optically thin cells with alignment layers of standard thickness (e.g. 20 nm). We investigate the phase lag limit for optically thin cells and also perform error propagation analysis to determine the accuracy of the estimated LC parameters. Our approach allows us to characterise not only the LC material itself, but also the properties of a LC cell or device. We have used the CPI measurement method to reliably determine a range of parameters, such as splay and bend elastic constants, viscosities, cell thickness, pretilt and polar anchoring energy [21–23], in a single experiment, for several combinations of LCs and alignment layers. However, its correct operation relies on having the values of the LC refractive indices and dielectric coefficients as input parameters. If these parameters are missing or their values are only estimated, the error propagation analysis allows us to determine how reliable the CPI method is in determining the other, core LC parameters.

The structure of this paper is as follows. First, we present the optical setup, experimental techniques and methods. We then

explore the lowest phase lag limit for our CPI-based method in Section 3A. We characterise LCs with partially known dielectric coefficients and find the errors on the extracted LC parameters that arise from the uncertainty on the refractive indices and the dielectric coefficients in Section 3B. In the conclusions, we review our results and discuss the case of geometrically thin, but optically thick cells.

2. EXPERIMENTAL METHOD AND FITTING PROCEDURE

LC cell parameters can be extracted from reliable cross-polarised intensity measurements [17] using an Optical Multi-Parameter Analyser (OMPA) described in detail by Bennett et al. [21, 22]. We use planar LC cells with cell gaps of 10 µm to 12 µm, filled with nematic LCs, namely E7, MLC6815 and LC18523 from Merck. The alignment layers consist of polyimide (PI) or the photoconductive polymer polyvinylcarbazole (PVK) doped with fullerene C_{60}, deposited on electrodes made of indium tin oxide (ITO). The LC cells are placed between crossed polarisers at 45° to the optical axis of the LC, and the optical transmission of the system is recorded as a function of the AC voltage amplitude applied to the cell. A diagram of the experimental setup is presented in Figure 1.

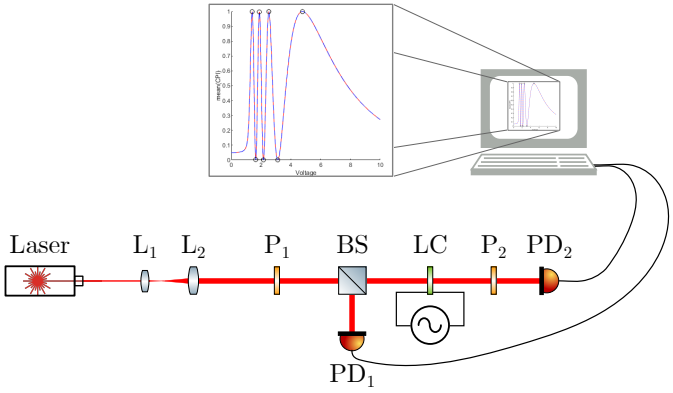

Fig. 1. Schematic representation of the experimental setup. The laser beam is expanded by the lenses L_1 and L_2 for analysis of the whole LC cell. The LC sample (LC), which is controlled by an AC voltage source, is placed between the polarisers P_1 and P_2. The beam splitter (BS) produces a reference beam detected by the reference photodetector PD_1 and a transmitted beam detected by the main photodetector PD_2. The measurement output is a plot of the CPI as a function of the voltage applied to the cell (insert).

During a computer-controlled CPI measurement, a voltage-dependent CPI trace is collected and is subsequently fitted in order to extract the LC properties. The standard fitting procedure requires a CPI trace with at least one minimum and one maximum in order to automatically normalise the data between 0 (smallest minimum) and 1 (largest maximum), which is equivalent to having a total phase lag larger than 2π. For cells that are either geometrically thin or contain low-birefringence LCs, i.e. cells with a phase lag smaller than 2π which we call henceforth "thin cells", this procedure is modified by measuring separately the minimum and maximum transmitted intensity. In order to record the minimum intensity, the LC sample is removed, so a configuration of crossed polarisers and no cell is used. The maximum intensity can be measured using parallel polarisers and an empty cell. With this normalisation of the CPI trace, the phase lag limit can be reduced to less than π.

The fitting procedure is based on the Frank–Oseen static theory of nematics, which is used to find the alignment equations of a nematic liquid crystal in electrostatic field. The time evolution of the director field of the liquid crystal, and the cross-polarised intensity, see Eq. (3), are computed in MATLAB as described by Bennett et al. [21, 22].

The fitting procedure requires the following LC parameters to be specified: the extraordinary and ordinary refractive indices, n_e and n_o respectively, and the dielectric coefficients $\varepsilon_{\parallel}$ and $\varepsilon_{\perp}$. In this paper we have determined the dielectric coefficients $\varepsilon_{\parallel}$ and $\varepsilon_{\perp}$ of MLC6815 for validation purposes by measuring the capacitance of a planar cell before and after it was filled using the auto balancing bridge method [24] and a DC voltage source.

3. RESULTS AND DISCUSSION

The CPI measurement method extracts the liquid crystal parameters from the phase lag experienced by a linearly polarised beam as it passes through a LC cell. This is measured as a function of voltage, thus probing and measuring the competing effect of the liquid crystal electric coupling and its elastic stiffness. The total phase lag $\Delta\Phi$ of the liquid crystal is given by [17]

$$\Delta\Phi = \frac{2\pi d \Delta n}{\lambda}, \tag{1}$$

where d is the cell thickness, λ the wavelength of the light propagating through the LC cell, and Δn is the cell effective birefringence, given by [21, 22]

$$\Delta n = \int_0^d \left[\frac{n_e n_o}{\sqrt{n_e^2 \sin^2\theta(z) + n_o^2 \cos^2\theta(z)}} - n_o \right] \mathrm{d}z\,. \tag{2}$$

Here we set the z-coordinate in the direction of the cell thickness; the cell is positioned between $z = 0$ and $z = d$, and $\theta(z)$ denotes the angle between the input surface and the director in the director alignment plane. Finally, the cross-polarised intensity is [17]

$$I = \sin^2\left(\frac{\Delta\Phi}{2}\right). \tag{3}$$

This equation shows that the CPI oscillates between 0 and 1, with each transition between two consecutive extrema corresponding to a decrease of the phase lag by π. Cells of decreasing thickness have smaller and smaller phase lags, which leads to fewer and fewer oscillations, and in the limiting case of a thin cell, which we consider here, the maximum phase lag is smaller than 2π so that there is at most one or, possibly, no extrema of the CPI. Figure 2 shows a comparison of CPI and phase lag traces between thick (10 µm) and thin (1 µm and 2 µm) E7 cells.

As discussed in the previous section, the CPI normalisation differs in thick and thin cells. In thick cells, where there are at least one maximum and one minimum of the CPI trace, the data can be normalised automatically. In thin cells, additional measurements of the minimum and maximum intensity are needed. One important aspect that needs to be considered here is the reliability of the thin cell normalisation method. The reliability can be compromised further if parameters like n_e, n_o, $\varepsilon_{\parallel}$ and $\varepsilon_{\perp}$ are only partially known. We address such reliability issues by looking into, separately, the errors on the fitting parameters stemming either from the process of normalisation or from the uncertainty over the values of the dielectric anisotropy and the birefringence.

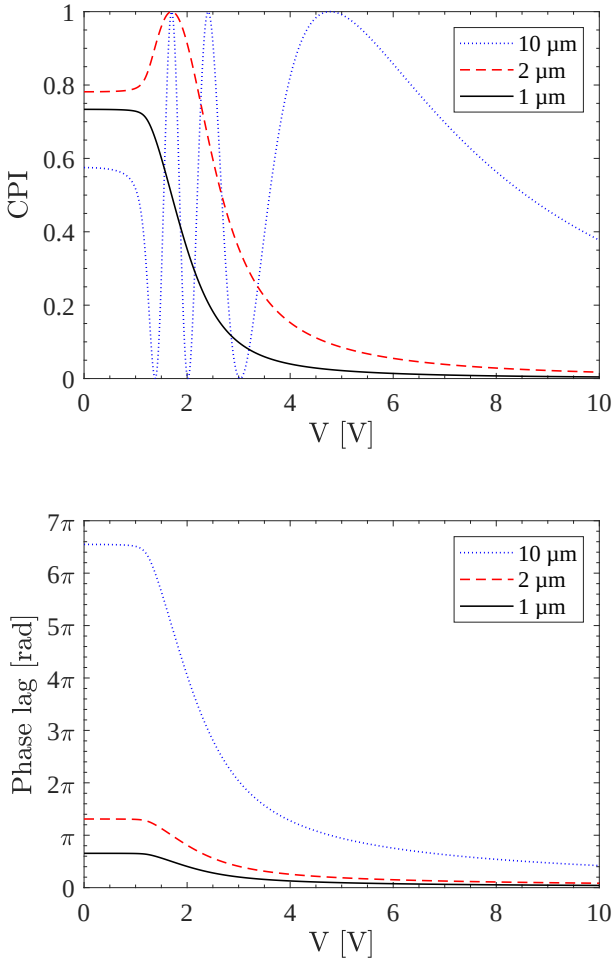

Fig. 2. Simulated cross-polarised intensity (top) and phase lag (bottom) of E7 cells with thickness of 1 µm, 2 µm and 10 µm. The LC cell parameters are: elastic constants $K_1 = 10.9$ pN and $K_3 = 17.895$ pN, dielectric coefficients $\varepsilon_{\parallel} = 19.54$ and $\varepsilon_{\perp} = 5.17$, pretilt $\theta_0 = 2°$, strong polar anchoring energy, i.e. $W_p = 1\,\mathrm{J/m^2}$, and refractive indices $n_e = 1.7287$ and $n_o = 1.5182$ at $\lambda = 642$ nm.

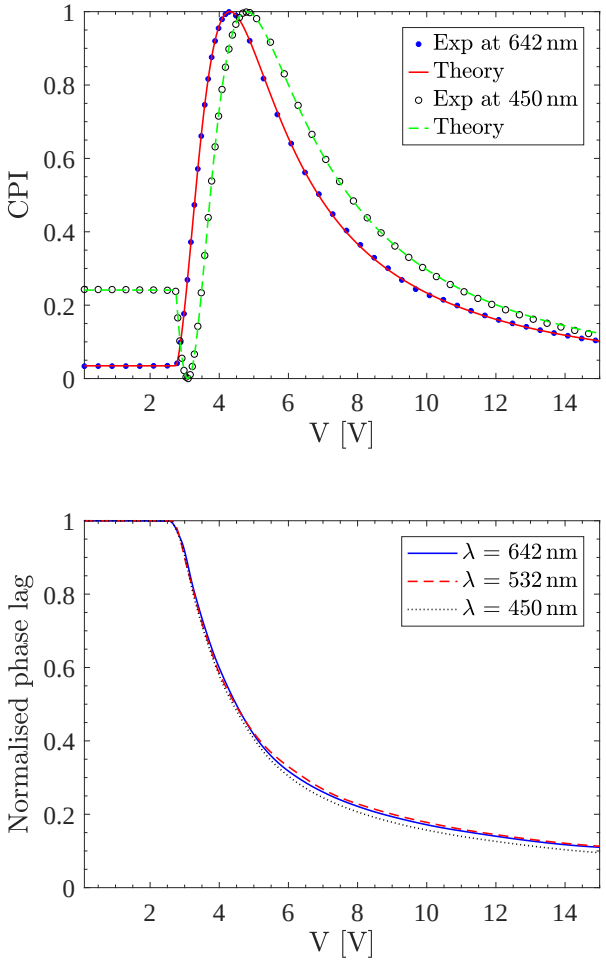

Fig. 3. Voltage-dependent CPI traces and theoretical fits (top) and normalised phase lag (bottom) for the LC18523 PI PVK:C_{60} cell at different wavelengths. Parameter values extracted from the CPI traces are presented in Table 1.

A. Thin cell measurements

Studying optically thin cells allowed us to investigate the limit of the CPI measurement method. In Figure 3 (top) we present a comparison between the two normalisation methods for the case of a low birefringence 12 µm-thick LC18523 cell with PI and PVK:C_{60} alignment layers. The CPI traces of the LC18523 cell were measured at three wavelengths: 450 nm, 532 nm and 642 nm. Using these three wavelengths allowed us to obtain data with three different values of the total phase lag (see Eq. (1)) and hence to compare thin-cell characterisation (at 642 nm) to thick-cell characterisation regime (at 450 nm and 532 nm) for the same cell. In Figure 3 (top) the CPI traces for the shortest and longest wavelength are shown, while the 532 nm curve has been omitted for clarity. For the shortest wavelength (empty circles in Figure 3 (top)) the maximum phase lag is larger than 2π and the CPI data has both a maximum and a minimum, so automatic normalisation is possible. For the longest wavelength (filled circles) there is only one extremum, so we use the thin-cell normalisation method.

In all cases we obtain very good agreement between the fitting curves and the experimental data (see Figure 3 (top)). The parameter values obtained from the OMPA fits for the LC18523 cell at all three wavelengths are presented in Table 1, where the Fréedericksz transition threshold voltage at zero pretilt, V_{th}, is defined as [25]

$$V_{\mathrm{th}} = \pi\sqrt{\frac{K_1}{\varepsilon_0 \Delta\varepsilon}}. \qquad (4)$$

Here K_1 is the splay elastic constant, ε_0 is the permittivity of free space and $\Delta\varepsilon = \varepsilon_{\parallel} - \varepsilon_{\perp}$ is the dielectric anisotropy. The parameters extracted from the fitting, for example the elastic constants, show good agreement with the published values summarised in Table 2, thus, confirming that our method is sufficiently robust to characterise thin cell with a CPI containing just one extremum.

Interestingly at the shortest wavelength used, namely 450 nm, the anchoring energy is weaker than for the longer wavelengths. This small effect can also be seen in the graph of the normalised phase lag, Figure 3 (bottom), where at 450 nm the tail of the normalised phase lag curve is lower than than those at longer wavelengths. This result, which is likely to be associated with the increased photoconductivity of the aligning layer, PVK:C_{60}, in the blue region of the spectrum, is currently being studied and will be reported separately. For the purpose of the investigation

λ [nm]	V_{th} [V]	K_1 [pN]	K_3 [pN]	W_p [J/m^2]
642	1.96	8.6	10.9	1
532	1.91	8.2	11.8	1
450	1.96	8.6	10.7	6.8×10^{-5}

Table 1. Values of the threshold voltage V_{th}, the splay K_1 and bend K_3 elastic constants, and of the polar anchoring energy W_p obtained by fitting the LC18523 PI PVK:C_{60} CPI traces in Figure 3 with OMPA. Here $W_p = 1\,\mathrm{J/m^2}$ corresponds to infinitely strong polar anchoring energy.

presented here we note, however, that the OMPA method is capable of detecting small changes in anchoring even in thin cells.

As a further comparison, the automatic and thin-cell normalisation methods were applied to the same CPI experimental data of a MLC6815 cell with one maximum and one minimum. No noticeable difference between the results of the two normalisation processes was discovered.

The thin-cell normalisation method was tested experimentally only for CPI traces with no minima. Cells that are optically very thin, i.e. with a maximum phase lag smaller than π, can in principle be measured using the thin-cell normalisation of the CPI data. In this case, however, due care must be taken to account for reflection and absorption in the LC cell when estimating the maximum intensity. If the cells are geometrically thin as well, their effective birefringence and voltage threshold may depend on the cell thickness [31, 32], and their response time may be longer under weak anchoring [20, 33]. Therefore, it may also be necessary to include the inert layer corrections discussed by Wu and Efron in [32].

B. Partially characterised liquid crystals

New LC mixtures and experimental composite LCs are often accompanied only by their birefringence and dielectric anisotropy values. We explore the impact of this uncertainty in the actual magnitudes of their indices on the reliability of our CPI characterisation method. The LC alignment depends on the values of $\varepsilon_{\parallel}$ and $\varepsilon_{\perp}$, but not on the refractive indices. Only the cross-polarised intensity depends on the refractive indices. More specifically, the phase lag depends primarily on the birefringence and only more weakly on the exact values of the refractive indices, see Eq. (1)-Eq. (3). Therefore, when fitting data with large uncertainties on the refractive indices or the dielectric coefficients, we expect relatively small impact from the unknown refractive indices n_e, n_o, providing the birefringence $\Delta n = n_e - n_o$ is known. However, bigger errors are expected when the dielectric coefficients $\varepsilon_{\parallel}$ and $\varepsilon_{\perp}$ are unknown, even if the dielectric anisotropy $\Delta\varepsilon = \varepsilon_{\parallel} - \varepsilon_{\perp}$ is known.

On the strength of these observations, we consider first the effect of partly characterised dielectric coefficients. We assume that the refractive indices and the dielectric anisotropy, $\Delta\epsilon$, are known, but not the individual values of $\varepsilon_{\parallel}$ and $\varepsilon_{\perp}$. In this case, one can formulate reasonable guesses for these parameters in order to fit the data. The results of such estimations are presented in Figure 4, where the literature value for $\varepsilon_{\perp}$ is 5.17 for E7, while for MLC6815 we measured $\varepsilon_{\perp} = 4.3$ at room temperature. Indeed, as can be observed, the fittings with these values of the dielectric coefficient are the closest to the experimental data for each LC; values further away from the true value of $\varepsilon_{\perp}$ give worse and worse fits and in some cases convergence of the fitting algorithm cannot be reached. Based on how close the fitting curves in Figure 4 are to each other for each LC cell, the quality of the fit cannot be used to determine the values of the dielectric constants. However, we can conclude that the fit is poor if $\epsilon_{\perp}$ is over- or under-estimated by a factor of at least two. The parameter values obtained from the fitting procedure using different values of $\epsilon_{\perp}$ are given in Table 3. The results for the elastic constants of E7 using the correct value $\varepsilon_{\perp} = 5.17$ are well within the accepted range of the literature values given in Table 2. Interestingly, as the results in Table 3 suggest, the elastic constants are somewhat insensitive to the precise values of $\varepsilon_{\parallel}$ and $\varepsilon_{\perp}$. Reducing $\varepsilon_{\perp}$ by a factor of two with respect to the accepted value of $\varepsilon_{\perp}$ gives up to 20% error on the elastic constants, while doubling the accepted value of $\varepsilon_{\perp}$ gives up to 12% error on the elastic constants. Therefore, even with some uncertainty over the dielectric coefficients, the elastic constants can be estimated reasonably well.

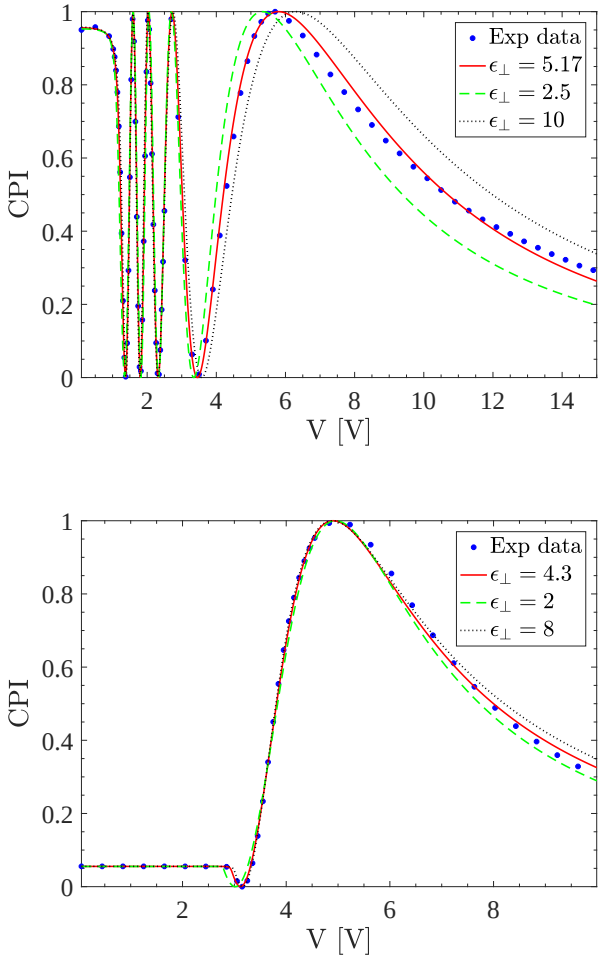

Fig. 4. Theoretical fits using different $\varepsilon_{\perp}$ values for an E7 cell (top) and a MLC6815 cell (bottom) at 532 nm. The corresponding values of $\varepsilon_{\parallel}$ were obtained using the dielectric anisotropy $\Delta\varepsilon$ reported in the literature and summarised in Table 2. The parameter values extracted from the fitting procedure are presented in Table 3.

We now address the more general case of estimating the error on the fitted parameters in terms of the error on the refractive indices and the dielectric permittivities. In other words, we

LC	$\varepsilon_{\parallel}$	$\varepsilon_{\perp}$	n_e	n_o	λ [nm]	V_{th} [V]	K_1 [pN]	K_3 [pN]
E7	19.54*	5.17*	1.7287 [26]	1.5182 [26]	642	0.90	10.5 [27]	12.3 [16]
						0.95	11.7 [28]	19.5 [28]
TL205	8.68 [29]	4.01 [29]	1.7317 [30]	1.5205 [30]	642	2.03	17.2 [29]	20.2 [29]
LC18523	6.7 [29]	4.2 [29]	1.5 [30]	1.453 [30]	642	1.87	7.85 [29]	10 [29]
MLC6815	6.9	4.3	1.5191*	1.4674*	589	2.07	10	12

Table 2. Literature values of the LC parameters for four standard LCs: E7, TL205, LC18523 and MLC6815. The wavelength at which the refractive indices are given is also specified. The threshold voltage V_{th} was computed using Eq. (4) and the corresponding value of K_1. The threshold voltage computed here may be different from published values for cells with non-zero pretilt. The MLC6815 parameters $\varepsilon_{\parallel}$, $\varepsilon_{\perp}$, K_1 and K_3 were measured in this work. The refractive indices n_e and n_o of TL205 and LC18523 were collected as part of the investigation presented by Warenghem et al. [30]. A range of values were found for the elastic constants of E7, so only the maximum and the minimum values are given for clarity. The listed parameters are used to calculate the errors in Tables 4 and 5, where for E7 we use $K_1 = 10.9$ pN and $K_3 = 17.895$ pN.
* Merck KGaA Technical data sheet, 2005

LC	$\varepsilon_{\perp}$	K_1 [pN]	K_3 [pN]
	2	8.1	14.4
	3	9.3	14.6
E7	**5.17**	**10.6**	**15.3**
	10	11.8	16.6
	12	12.1	17.0
	2	9.0	12.3
	4	10.0	12.0
MLC6815	**4.3**	**10.1**	**12.0**
	6	10.4	12.1
	8	10.6	12.3

Table 3. Fitting parameters for different estimates of $\varepsilon_{\perp}$ and $\varepsilon_{\parallel} = \varepsilon_{\perp} + \Delta\varepsilon$ obtained using OMPA for E7 and MLC6815 cells for fixed dielectric anisotropy $\Delta\varepsilon$. We have used the literature values of $\Delta\epsilon$ reported in Table 2. Graphical representation of the fits is given in Figure 4.

consider the case when all the optical and electrical LC parameters are known, but only within a certain uncertainty range. How do these uncertainties affect the CPI-based estimate of the other liquid crystal parameters? In this analysis we use the standard error propagation formulas, with the added factor that the relation between the known and the fitting parameters is known only in implicit form through the fitting procedure. We therefore must use the implicit function theorem to evaluate the derivatives of the fitting parameters in terms of the dielectric permittivities and the refractive indices. The details of the method can be found in Appendix A.

The relative errors for four LC cells used to compare the case of unknown refractive indices to that of unknown dielectric permittivities are presented in Tables 4 and 5. The LC parameters used in our calculations are given in Table 2. Comparison between Table 4 and Table 5 suggests that measurements of the properties of a liquid crystal with refractive indices with 10% error, $\Delta n_o = \Delta n_e = 0.1\, n_o$, and fixed birefringence can give reliable results with typical errors below 0.02% for all of the fitting parameters K_1, K_3, d, θ_0 and W_p for the four LCs. These errors are negligible when compared to experimental noise or numerical errors during the fitting procedure. In contrast, measurements of the properties of a liquid crystal with dielectric permittivities with 10% error, $\Delta\epsilon_{\perp} = \Delta\epsilon_{\parallel} = 0.1\,\epsilon_{\perp}$, and fixed dielectric anisotropy give errors ranging from 0.02% to 16%. In this case the errors are significant, so the reliability of the results is considerably worse. The pretilt, followed by the elastic constants, is the most sensitive parameter to errors on the dielectric coefficients, while the cell thickness is the least sensitive parameter. Similar behaviour is observed for infinitely strong anchoring. These results confirm that unknown refractive indices n_e, n_o and fixed birefringence $\Delta n = n_e - n_o$ lead to much smaller errors than unknown dielectric coefficients $\varepsilon_{\parallel}$, $\varepsilon_{\perp}$ and fixed dielectric anisotropy $\Delta\varepsilon = \varepsilon_{\parallel} - \varepsilon_{\perp}$. This is in agreement with the preliminary analysis at the beginning of this section.

It is important to note here that when the CPI is close to 0 or 1 (i.e. $\Delta\Phi = m\pi$) at $V = 0$, the CPI is less sensitive to changes in the phase lag. Therefore, there is more freedom for the fitting parameters due to the weaker constraints, hence bigger errors are expected. This is confirmed by the error propagation analysis in Appendix A. The dependence of the error of the splay elastic constant on the maximum phase lag, i.e. the phase lag at $V = 0$, is shown in Figure 5 as an example. It clearly indicates that when the maximum phase lag is an integer multiple of π, i.e. when the CPI at $V = 0$ is close to either 0 or 1, the error is largest. This behaviour is typical of most of the fitting parameters. Therefore, in order to minimise the error on the fitting parameters, it is important to choose a cell thickness or a light wavelength such that the maximum phase lag is different from an integer multiple of π.

4. CONCLUSION

In this work, we considered two technologically important constraints for liquid crystal devices: thin cells/small phase lag and liquid crystals with incomplete set of dielectric and refractive indices.

The LC parameters of optically thin cells were successfully extracted from cross-polarised intensity data with a limit of the total phase lag of $\Delta\Phi \approx \pi$. The measurement procedure proposed here is also valid for cells that are geometrically very thin, and if their boundary effects become significant [32], effective

LC	ΔK_1 [%]	ΔK_3 [%]	Δd [%]	$\Delta\theta_0$ [%]	$\Delta ln(W_p)$ [%]
E7	0.0065	0.0099	0.0002	0.0206	0.0025
TL205	0.0023	0.0143	0.0002	0.0067	0.0016
LC18523	0.0003	0.0036	0	0.0009	0.0012
MLC6815	0.0006	0.0036	0.0005	0.0112	0.0009

Table 4. Relative errors on the fitting parameters for fixed birefringence and absolute error on the refractive indices $\Delta n_o = \Delta n_e = 0.1\, n_o$ for four LCs. The maximum amplitude of the applied voltage is $V_{max} = 10V$ for E7, LC18523 and MLC6815, and $V_{max} = 20V$ for TL205. The errors are estimated using Eq. (9). The liquid crystal parameters used are listed in Table 2. The other parameters are $d = 12\,\mu$m, $\theta_0 = 2°$, $W_p = 1 \times 10^{-4}\,$J/m^2, $\lambda = 642\,$nm for all cells.

LC	ΔK_1 [%]	ΔK_3 [%]	Δd [%]	$\Delta\theta_0$ [%]	$\Delta ln(W_p)$ [%]
E7	4.4	1.2	0.08	16.1	0.7
TL205	2.8	1.3	0.07	11.3	0.4
LC18523	1.4	2.2	0.02	4.3	1.6
MLC6815	1.8	2.1	0.04	7.6	1.3

Table 5. Relative errors on the fitting parameters for fixed dielectric anisotropy and absolute error on the dielectric coefficients $\Delta\epsilon_\perp = \Delta\epsilon_\parallel = 0.1\,\epsilon_\perp$ for four LCs. All LC cell parameters are as in Table 4.

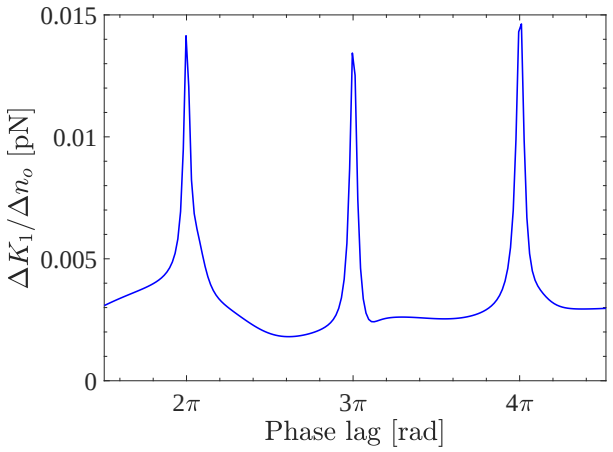

Fig. 5. Absolute error on the splay elastic constant K_1 divided by the uncertainty on the ordinary refractive index n_o as a function of the phase lag at V=0 V for E7 cell with varying thickness. The LC cell parameters are: elastic constants $K_1 = 10.9\,$pN and $K_3 = 17.895\,$pN, dielectric coefficients $\varepsilon_\parallel = 19.54$ and $\varepsilon_\perp = 5.17$, pretilt $\theta_0 = 2°$, strong polar anchoring energy $W_p = 1\,$J/m^2, and refractive indices $n_e = 1.7287$ and $n_o = 1.5182$ at $\lambda = 642\,$nm.

cell parameters may still be extracted [20].

Furthermore, we have demonstrated the reliability of our approach, using the associated error analysis, to determine elastic constants for LCs with unknown refractive indices and/or unknown dielectric coefficients. In the former case, the uncertainty on the refractive indices does not affect significantly the accuracy of the extracted elastic constants; in the latter case, a reasonably good approximation can be obtained for the elastic constants. The error analysis is based on using the implicit function theorem in the standard error propagation formula. In this paper we have applied it to a Frank-Oseen model for a planar cell, but it can also be used for twist cells and for cells where flow effects are significant, the latter being modelled using an Ericksen-Leslie theory [34, 35]. The combination of thin-cell fitting and error analysis presented here is quite versatile and can serve as a useful aid in efficient assessment of new liquid crystals in technologically-relevant geometries.

A. ERROR PROPAGATION

The OMPA fitting procedure returns a set of *fitting* parameters, K_1, K_3, d, θ_0 and W_p, by fitting the experimental CPI trace, provided that n_e, n_o, $\varepsilon_\parallel$ and $\varepsilon_\perp$ are *known*. Let $\boldsymbol{x}$ and $\boldsymbol{y}$ denote the known and fitting parameter vectors respectively,

$$\boldsymbol{x} = \left(n_e\; n_o\; \varepsilon_\parallel\; \varepsilon_\perp\right)^T, \quad \boldsymbol{y} = \left(K_1\; K_3\; d\; \theta_0\; W_p\right)^T. \tag{5}$$

The fitting procedure in OMPA finds $\boldsymbol{y}$ by minimising the distance $D(\boldsymbol{x}, \boldsymbol{y})$ between the experimental and the theoretical CPI traces, by solving the system of algebraic equations

$$F_i(\boldsymbol{x}, \boldsymbol{y}) \equiv \frac{\partial D^2(\boldsymbol{x}, \boldsymbol{y})}{\partial y_i} = 0. \tag{6}$$

The absolute error on the fitting parameters is given by the standard error propagation formula

$$\Delta y_i = \left|\frac{\partial y_i(\boldsymbol{x})}{\partial x_j}\right| \Delta x_j, \tag{7}$$

where the Einstein summation convention is assumed, and Δx_j and Δy_i denote the absolute errors on x_j and y_i respectively. We compute the derivative using the Implicit function theorem

$$\frac{\partial y_i}{\partial x_j} = -\left[\frac{\partial F_k}{\partial y_i}\right]^{-1}\left[\frac{\partial F_k}{\partial x_j}\right], \tag{8}$$

where $\left[\frac{\partial F_k}{\partial x_j}\right]$ and $\left[\frac{\partial F_k}{\partial y_i}\right]$ are the Jacobian of $\boldsymbol{F}$ with respect to $\boldsymbol{x}$ and $\boldsymbol{y}$ respectively, and $[\,]^{-1}$ denotes the matrix inverse. Substituting equations Eq. (6) and Eq. (8) into Eq. (7) we obtain that the error on the fitting parameters is given by

$$\Delta y_i = \left| \left[\frac{\partial^2 D^2(\boldsymbol{x},\boldsymbol{y})}{\partial y_i \partial y_k} \right]^{-1} \left[\frac{\partial^2 D^2(\boldsymbol{x},\boldsymbol{y})}{\partial x_j \partial y_k} \right] \right| \Delta x_j. \tag{9}$$

B. BACKMATTER

Funding. The authors acknowledge the financial support of the Leverhulme Trust (grant RPG-2019-055).

Acknowledgments. We would like to thank Tim Sluckin, Tetiana Orlova, Eleni Perivolari and Elena Ouskova for useful discussions that led to this work.

Disclosures. The authors declare no conflicts of interest.

Data availability. Data underlying the results presented in this paper are available from https://doi.org/10.5258/SOTON/D2125.

REFERENCES

1. Y. Zhang, J. Sun, Y. Liu, J. Shang, H. Liu, H. Liu, X. Gong, V. Chigrinov, and H. S. Kowk, "A flexible optically re-writable color liquid crystal display," Appl. Phys. Lett. **112**, 131902 (2018).
2. P. F. Bai, R. A. Hayes, M. Jin, L. Shui, Z. C. Yi, L. Wang, X. Zhang, and G. Zhou, "Review of paper-like display technologies (Invited Review)," Prog. In Electromagn. Res. **147**, 95–116 (2014).
3. S. Oka, T. Sasaki, T. Tamaru, Y. Hyodo, L. Jin, S. Takayama, and S. Komura, "9-2: Optical Compensation Method for Wide Viewing Angle IPS LCD Using a Plastic Substrate," SID Symp. Dig. Tech. Pap. **47**, 87–90 (2016).
4. J. Xiong and S.-T. Wu, "Planar liquid crystal polarization optics for augmented reality and virtual reality: from fundamentals to applications," eLight **1**, 3 (2021).
5. Y. Iwashita, Y. Umezu, S. Kawakami, K. Takeuchi, T. Kusumoto, S. Takehara, and H. Takatsu, "Liquid Crystal Mixtures with Low Birefringence for Active-Matrix LCD," Mol. Cryst. Liq. Cryst. **411**, 41–48 (2004).
6. O. Buchnev, N. Podoliak, K. Kaltenecker, M. Walther, and V. A. Fedotov, "Metasurface-Based Optical Liquid Crystal Cell as an Ultrathin Spatial Phase Modulator for THz Applications," ACS Photonics **7**, 3199–3206 (2020).
7. Q. Liu, Y. Yuan, and I. I. Smalyukh, "Electrically and Optically Tunable Plasmonic Guest–Host Liquid Crystals with Long-Range Ordered Nanoparticles," Nano Lett. **14**, 4071–4077 (2014).
8. A. Chaudhary, R. Shukla, P. Malik, R. Mehra, and K. Raina, "ZnO/FLC nanocomposites with low driving voltage and non-volatile memory for information storage applications," Curr. Appl. Phys. **19**, 1374–1378 (2019).
9. A. Chaudhary, P. Malik, R. Shukla, R. Mehra, and K. Raina, "Role of SiO_2 optically active mediators to tailor optical and electro-optical properties of ferroelectric liquid crystalline nanocomposites," J. Mol. Liq. **314**, 113580 (2020).
10. C. Hamon, E. Beaudoin, P. Launois, and E. Paineau, "Doping Liquid Crystals of Colloidal Inorganic Nanotubes by Additive-Free Metal Nanoparticles," The J. Phys. Chem. Lett. **12**, 5052–5058 (2021).
11. Z. Mai, Y. Yuan, J.-S. B. Tai, B. Senyuk, B. Liu, H. Li, Y. Wang, G. Zhou, and I. I. Smalyukh, "Nematic Order, Plasmonic Switching and Self-Patterning of Colloidal Gold Bipyramids," Adv. Sci. p. 2102854 (2021).
12. N. Brouckaert, N. Podoliak, T. Orlova, D. Bankova, A. F. De Fazio, A. G. Kanaras, O. Hovorka, G. D'Alessandro, and M. Kaczmarek, "Nanoparticle-Induced Property Changes in Nematic Liquid Crystals," Nanomaterials **12**, 341 (2022).
13. V. Fréedericksz and V. Zolina, "Forces causing the orientation of an anisotropic liquid," Trans. Faraday Soc. **29**, 919–930 (1933).
14. G.-P. Chen, H. Takezoe, and A. Fukuda, "Determination of K_i (i = 1–3) and μ_j (j = 2–6) in 5CB by observing the angular dependence of Rayleigh line spectral widths," Liq. Cryst. **5**, 341–347 (1989).
15. A. A. Joshi, J. K. Whitmer, O. Guzmán, N. L. Abbott, and J. J. de Pablo, "Measuring liquid crystal elastic constants with free energy perturbations," Soft Matter **10**, 882–893 (2014).
16. B. Klus, U. A. Laudyn, M. A. Karpierz, and B. Sahraoui, "All-optical measurement of elastic constants in nematic liquid crystals," Opt. Express **22**, 30257 (2014).
17. S.-T. Wu, U. Efron, and L. D. Hess, "Birefringence measurements of liquid crystals," Appl. Opt. **23**, 3911 (1984).
18. M. Bharath Kumar, M. Awwal Adeshina, D. Kang, Y. Jee, T. Kim, M. Choi, and J. Park, "Enhancement of Birefringence in Reduced Graphene Oxide Doped Liquid Crystal," Nanomaterials **10**, 842 (2020).
19. X. Zhao, T. Li, Z. Tang, Y. Li, Y. Miao, H. Xing, M. Cai, X. Wang, X. Kong, and W. Ye, "Accurate determination on the pre-tilt angle of liquid crystal cell by combining optical and electrical measurement," Liq. Cryst. **48**, 15–22 (2021).
20. M. Jiao, Z. Ge, Q. Song, and S.-T. Wu, "Alignment layer effects on thin liquid crystal cells," Appl. Phys. Lett. **92**, 061102 (2008).
21. T. Bennett, M. Proctor, M. Kaczmarek, and G. D'Alessandro, "Lifting degeneracy in nematic liquid crystal viscosities with a single optical measurement," J. Colloid Interface Sci. **497**, 201–206 (2017).
22. T. Bennett, M. Proctor, J. Forster, E. Perivolari, N. Podoliak, M. Sugden, R. Kirke, T. Regrettier, T. Heiser, M. Kaczmarek, and G. D'Alessandro, "Wide area mapping of liquid crystal devices with passive and active command layers," Appl. Opt. **56**, 9050 (2017).
23. E. Perivolari, G. D'Alessandro, V. Apostolopoulos, N. Brouckaert, T. Heiser, and M. Kaczmarek, "Two-dimensional snapshot measurement of surface variation of anchoring in liquid crystal cells," Liq. Cryst. pp. 1–11 (2021).
24. L. M. Blinov, "Magnetic, Electric and Transport Properties," in *Structure and Properties of Liquid Crystals,* (Springer, Dordrecht, 2011), pp. 151–187.
25. I. W. Stewart, *The Static and Dynamic Continuum Theory of Liquid Crystals* (CRC Press, 2004), 1st ed.
26. J. Li, C.-H. Wen, S. Gauza, R. Lu, and S.-T. Wu, "Refractive Indices of Liquid Crystals for Display Applications," J. Disp. Technol. **1**, 51–61 (2005).
27. C. L. Trabi, C. V. Brown, A. A. T. Smith, and N. J. Mottram, "Interferometric method for determining the sum of the flexoelectric coefficients (e1+e3) in an ionic nematic material," Appl. Phys. Lett. **92**, 223509 (2008).
28. H. Wang, T. X. Wu, S. Gauza, J. R. Wu, and S. Wu, "A method to estimate the Leslie coefficients of liquid crystals based on MBBA data," Liq. Cryst. **33**, 91–98 (2006).
29. N. Podoliak, O. Buchnev, M. Herrington, E. Mavrona, M. Kaczmarek, A. G. Kanaras, E. Stratakis, J.-F. Blach, J.-F. Henninot, and M. Warenghem, "Elastic constants, viscosity and response time in nematic liquid crystals doped with ferroelectric nanoparticles," RSC Adv. **4**, 46068–46074 (2014).
30. M. Warenghem, J. F. Henninot, J. F. Blach, O. Buchnev, M. Kaczmarek, and M. Stchakovsky, "Combined ellipsometry and refractometry technique for characterisation of liquid crystal based nanocomposites," Rev. Sci. Instruments **83**, 035103 (2012).
31. S. Wu and U. Efron, "Electro-Optic Behavior Of Thin Nematic Liquid Crystal Cells," in *Nonlinear Optics and Applications,* vol. 0613 (SPIE, 1986), p. 172.
32. S. Wu and U. Efron, "Optical properties of thin nematic liquid crystal cells," Appl. Phys. Lett. **48**, 624–626 (1986).
33. X. Nie, R. Lu, H. Xianyu, T. X. Wu, and S.-T. Wu, "Anchoring energy and cell gap effects on liquid crystal response time," J. Appl. Phys. **101**, 103110 (2007).
34. J. L. Ericksen, "Conservation laws for liquid crystals," Transactions Soc. Rheol. **5**, 23–34 (1961).
35. F. M. Leslie, "Some constitutive equations for liquid crystals," Arch. for Ration. Mech. Analysis **28**, 265–283 (1968).